

Visualizing Multiwavelength Astrophysical Data

Hongwei Li, *Student Member, IEEE*, Chi-Wing Fu, *Member, IEEE*, and Andrew J. Hanson, *Member, IEEE*

Abstract— With recent advances in the measurement technology for allsky astrophysical imaging, our view of the sky is no longer limited to the tiny visible spectral range over the 2D Celestial sphere. We now can access a third dimension corresponding to a broad electromagnetic spectrum with a wide range of allsky surveys; these surveys span frequency bands including long wavelength radio, microwaves, very short X-rays, and gamma rays. These advances motivate us to study and examine multiwavelength visualization techniques to maximize our capabilities to visualize and exploit these informative image data sets. In this work, we begin with the processing of the data themselves, uniformizing the representations and units of raw data obtained from varied detector sources. Then we apply tools to map, convert, color-code, and format the multiwavelength data in forms useful for applications. We explore different visual representations for displaying the data, including such methods as textured image stacks, the horseshoe representation, and GPU-based volume visualization. A family of visual tools and analysis methods is introduced to explore the data, including interactive data mapping on the graphics processing unit (GPU), the mini-map explorer, and GPU-based interactive feature analysis.

Index Terms—Astrophysical visualization, multiwavelength data, astronomy.

1 INTRODUCTION

Over thousands of years, astronomers have observed and studied the night sky within the range of visible light; it is now known that the light observable by the human eye covers just a very tiny fraction of the entire measurable electromagnetic spectrum. With the development of spectroscopy in 1814 by Joseph Fraunhofer, scientists began to study the electromagnetic waves as a function of their spectra, and astronomers began to search for effective methods to observe the sky in different wavelengths. However, only in recent decades have we had access to very large ground-based telescopes, designed for the measurement of long radio waves as well as optical light from outer space, and orbiting satellites especially designed to detect the parts of the electromagnetic spectrum that are blocked by the upper atmosphere (e.g., the ROSAT Project, a space mission dedicated to measuring X-rays). Astronomical observers all over the world now focus on Earth-based and space-based observations of portions of the electromagnetic spectrum invisible to the human eye. Many of these observing missions are “allsky surveys” that attempt to cover a major portion of the entire Celestial sphere.

These advances open a new window for us to observe and depict the two-dimensional sky; we can regard the electromagnetic spectrum as a third observable dimension in addition to the coordinates on the 2D Celestial sphere. Astrophysical objects have widely varying physical characteristics, and these manifest themselves in enormously different signatures in their electromagnetic emission features, intensities, and wavelengths. A given astrophysical object can be invisible in one wavelength range and while shining brilliantly in another. These interesting phenomena provide astronomers with significant hints about the origin, history, and behavior of astrophysical objects and materials.

Current practice for examining multiwavelength data typically involves creating false-color images and comparing images side-by-side to search for significant features and correlations. Since data with different wavelengths are produced by different research groups, a variety of color maps and different data mappings are applied to the raw data, while the raw data themselves are recorded in a variety of incompati-

ble formats and units from different detector technologies. The differences hinder flexible and intuitive visual comparison and data exploration. In addition, with recent advances in measurement technology, both the quality and the quantity of allsky surveys are continually increasing; the most recent survey data have higher angular precision, a wider range and precision of wavelengths, and higher dynamic range. Some survey data contain multiple images, each covering a specific frequency band. These advances further increase the amount of multi-spectral image data being collected and motivate us to investigate more efficient and effective visualization techniques applicable to the increasingly large volume of available data.

In this paper, we discuss first the acquisition of raw allsky data in various spectra, and then we propose the following visualization workflow to present and explore multiwavelength astronomical data:

- **GPU-based Data Processing:** This step includes data conversion, data mapping, color coding, and transfer function selection, with the purpose of creating consistent representations of allsky data obtained from different sources.
- **Multiwavelength Data Presentations:** This step includes the creation of a number of visual representations for presenting multi-wavelength data, including textured image stacks, the horseshoe representation, and GPU-based volume visualization.
- **Multiwavelength Visual Exploration:** This step includes the development of a set of interactive tools for exploring multiwavelength data: an interactive data mapping tool, the mini-map explorer, and a GPU-based interactive feature analysis toolbox.

Paper organization After reviewing related work on astronomical visualization in the next part of this section, we itemize in Section 2 the unique characteristics of multiwavelength astronomical data. The next three sections focus on the three components noted above: Section 3 details the data processing pipeline, Section 4 describes our visual representations for presenting the allsky data, and Section 5 describes our interactive visualization tools for exploring and analyzing the data. Finally, Section 6 presents the implementation details and examples of multiwavelength visualization results, while Section 7 contains concluding remarks.

Related Work Computer graphics and visualization techniques have long been used in the visualization of astronomical data. One early pioneering example is Blinn’s set of “Voyager Fly-by Animations” [3] produced by the NASA Jet Propulsion Laboratory. This series of animations illustrates various space missions including the Voyager 2 fly-by of Jupiter and the Pioneer 11 fly-by of Saturn.

Among relevant astronomical visualization work we note that of Gooch [17], who proposed different shading methods for data ob-

-
- Hongwei Li is with the Hong Kong University of Science & Technology, E-mail: lih@ust.hk
 - Chi-Wing Fu is with the Nanyang Technological University, Singapore E-mail: cwfu@ntu.edu.sg
 - Andrew J. Hanson is with Indiana University, Bloomington, E-mail: hanson@cs.indiana.edu

Manuscript received 31 March 2008; accepted 1 August 2008; posted online 19 October 2008; mailed on 13 October 2008.

For information on obtaining reprints of this article, please send e-mail to: tvcg@computer.org.

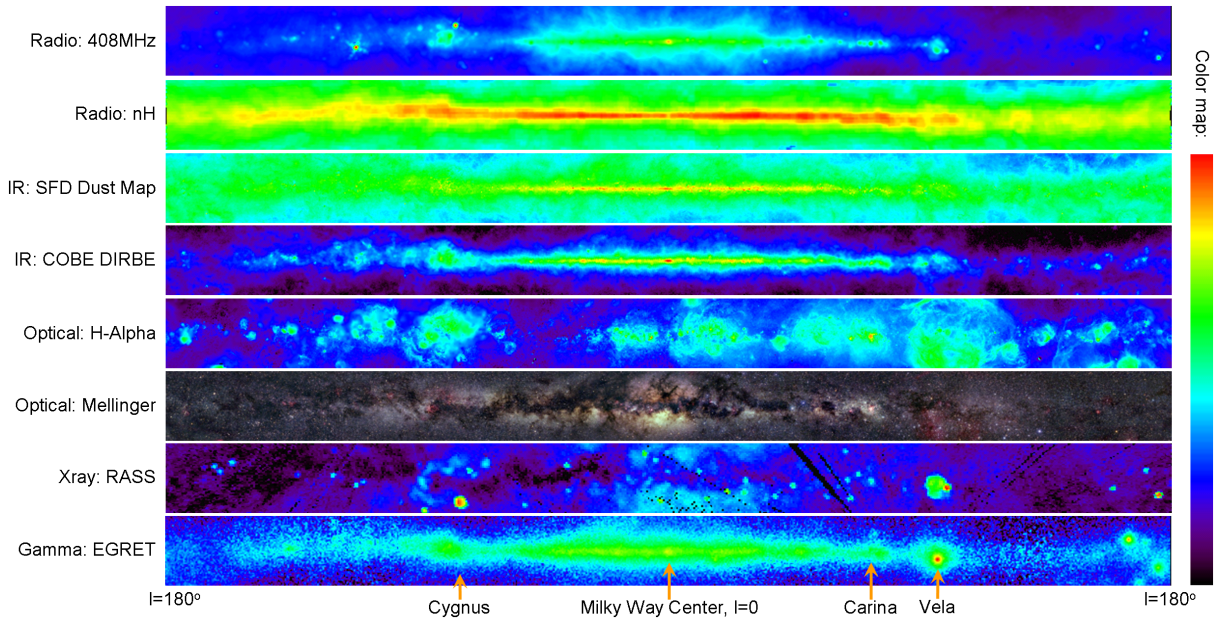


Fig. 1. Multiwavelength data centered at the Milky Way core, covering 360×25 degrees. The Galactic longitude l increases to the left from its origin at the image center.

Table 1. Allsky surveys: Example Multiwavelength Astrophysical Data

Survey name	EM range	Frequency	Wavelength	Measured Data Unit	Resolution	Coverage	Reference
408MHz	Radio	408 MHz	$7.3E-1$ m	degrees Kelvin	0.85 degrees	allsky	Haslam et al. [23]
nH (Neutral H)	Radio	1420 MHz	$2.1E-1$ m	atoms/cm ²	1 degree	allsky	Dickey and Lockman [8, 22]
SFD Dust Map	Infrared	3 THz	$1E-4$ m	MegaJanskys/steradian	0.1 degrees	allsky	Schlegel et al. [48]
COBE DIRBE	Infrared	1.25-240 THz	$1.3E-6 - 2.4E-4$ m	MegaJanskys/steradian	0.75 degrees	allsky	Hauser et al. [24]
Mellinger	Optical	428-750 THz	$4E-7 - 7E-7$ m	scaled intensity	0.025 degrees	allsky	Mellinger [39]
H-Alpha	Optical	457 THz	$6.56E-7$ m	Rayleighs	0.1 degrees	allsky	Finkbeiner [12]
RASS	X-ray	$2.42E16 - 4.84E17$ Hz	$6.20E-10 - 1.24E-8$ m	10^{-6} counts/s	2 degrees	98% allsky	Snowden et al. [50]
EGRET	Gamma	$7.25E21 - 2.42E24$ Hz	$1.24E-16 - 4.13E-14$ m	count/cm ² /steradian/s	2 degrees	allsky	Hartman et al. [21]

tained from radio telescopes, Ostriker and Norman [47], who proposed a framework for simulating cosmology and reviewed the related requirements in high performance computing environments, Hanson et al. [18, 19], who proposed a visualization framework for illustrating the context of time in cosmological data, Nadeau et al. [15, 42], who simulated a fly-through of a volumetric model of the Orion Nebula [9], Baranoski et al. [1], who proposed a rendering method for simulating the Aurora Borealis (the Northern Lights), Jensen et al. [29], who devised a physically-based model to render the night sky as seen from Earth, Kahler et al. [31], who used a supercomputer and adaptive mesh rendering to simulate the life-span of a star, Hopf et al. [27], who developed a PCA-based splatting technique for rendering point-based data in dynamic galaxy models, and Magnor et al. [35, 36], who developed an inverse volume rendering method for constructing and rendering planetary nebulae and reflection nebulae.

In addition, Miller et al. [41] derived a visualization tool to reveal structures such as filaments and voids in the Horologium-Reticulum supercluster. Li et al. [34] developed a scalable WIM (world-in-miniature) user interface for facilitating the efficient exploration of large-scale astrophysical environments. Weiskopf et al. [52] applied visualization techniques as a tool to explain and illustrate various relativity effects such as gravitational lensing. Fu et al. [14] proposed a transparently scalable visualization architecture for modeling and rendering astronomical models across large-scale astrophysical spaces. Li et al. [33] designed and proposed an assortment of uncertainty visualization techniques to meet the unique characteristics of astronomical visualization, and Navratil et al. [46] developed a system to visualize and simulate cosmological point-based datasets. The closest efforts we aware of are those of [4] and [28], where Brugel et al. [4] examined only the multi-spectral data within a very limited spectral range, while Jacob et al. [28] mainly focused on the information extraction process. In contrast, we propose a more comprehensive and general visualization framework, and focus on a much broader spectral range.

2 MULTIWAVELENGTH ASTROPHYSICAL DATA

Figure 1 shows some example multiwavelength astrophysical image data [2, 5, 16]. Typical datasets are allsky image data, meaning that they cover the entire 4π radian solid angle of the sky. The value of each pixel in the data image records the energy response per unit area per unit time of the detection equipment when it receives light within certain spectral ranges. To make these values visualizable, these data are all color-coded by our visualization system using the same color map, shown on the right hand side; for detailed descriptions of their physical properties, see Table 1. It is worthwhile noting that in making Figure 1, we crop the central region in the allsky images centered at the Milky Way core, with ranges 360×25 degrees in Galactic coordinates [6]. See Figure 2 for a summary of the Galactic coordinate system.

After describing the data, we summarize some unique characteristics (properties and features) of multiwavelength astrophysical data and contrast them with other image-by-image visualization domains, such as video visualization [7] (stack of continuous time frames), or medical visualization (stack of consecutive image scans):

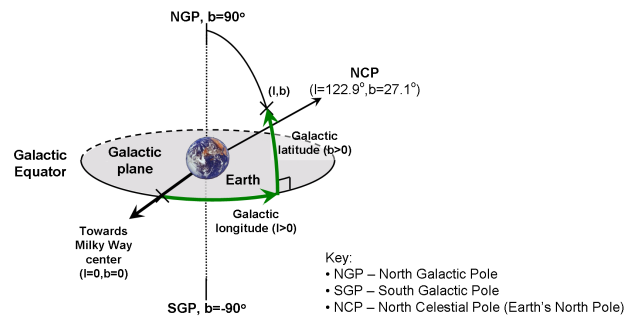


Fig. 2. The Galactic coordinate system: longitude l and latitude b .

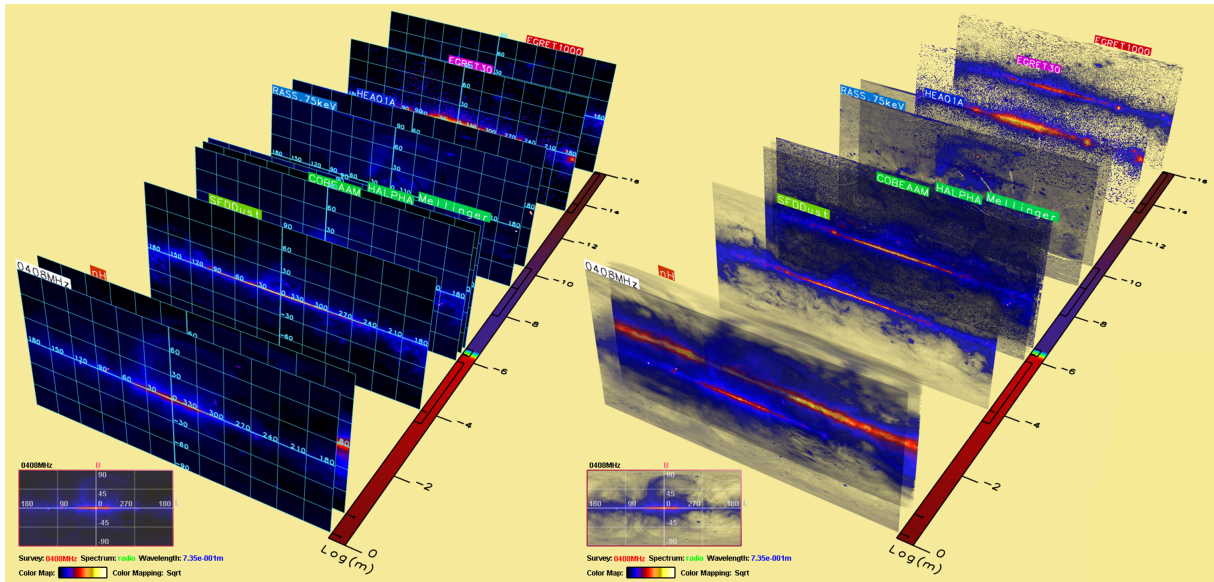


Fig. 3. Image-stack model. (Left) With Galactic coordinate grid but no transfer function. (Right) With transfer function enabled. The tags attached to the images indicate the data source. Moreover, we show also a color map on the right of the image stack to highlight the visible range location.

- **Discontinuity** Due to its physical properties, the third dimension (frequency or wavelength in the electromagnetic spectrum) of the image representation in the multiwavelength astrophysical data is encoded with an exponential scale; the data are arranged in small discrete ranges because the measuring apparatus can only cover a limited range of the electromagnetic spectrum at one time. This property is very different from the continuity and homogeneity in video data (temporal) and medical data (spatial).
- **Large data range** Since the physical composition of actual astronomical objects strongly influences their signature in different parts of the EM spectrum, the pixel response (at the same image location, galactic coordinate (l, b)) could be quite different in different frequency ranges; for example, Cygnus, see Figure 1, is a strong source of X-rays (because of its central black hole, Cygnus X-1), but it is weak at the other parts in the spectrum. Therefore, the data/feature correlation is not straightforward.
- **Different measurement units** Since different measuring devices are needed for acquiring data in different parts of the EM spectrum, the physical units of measured data typically vary (see Table 1); data conversion is needed to normalize the input data.

3 DATA PROCESSING PIPELINE

After downloading the allsky raw data, e.g., from [38], we carry out the following four steps to process the data before the visualization step. These are required because the raw data have high dynamic range (typically 32-bit floating point precision in the FITS image file format) and are recorded with diverse physical units.

Data conversion First, we apply appropriate transformation formulas to convert the raw data to a uniform physical unit that we choose as flux density in MegaJanskys (MJy); this is a tedious task because of the diversity of common data formats. See the Appendix for the conversion formulas.

Data mapping The second step is similar to tone mapping in high dynamic range imaging because we also have to convert the float values to an 8-bit display. In detail, this step includes: 1) threshold converted data values (some surveys contain invalid pixel values of certain pixel regions, e.g., the RASS X-ray data), 2) compute min/max and normalize the data values to the range $[0, 1]$, and 3) apply data mappings, for example, *linear*, *sqrt*, and *log* (with user parameters), where these are standard maps commonly used by astronomers. Note that since we have already converted all multiwavelength data into the same physical units, we can either *globally rescale* all data (with a global min/max) or *locally rescale*

each image data collection individually to the range $[0, 1]$. Though the global rescaling mechanism seems to be a reasonable choice to compare data across wavelength ranges, we may lose the capability to do relative comparison; for example, if we have a strong X-ray source, is it strong at other wavelengths relative to comparable objects? This is challenging because the flux density varies exponentially rapidly across wavelengths, e.g., the ratio between the flux density of infra-red light and gamma rays can be as large as 15 orders of magnitude [40].

Color mapping After mapping the data to the normalized range $[0, 1]$, we can apply color maps (or grey scale pseudocolor maps) to shade the image data. In practice, different color maps are used by astronomers working on different parts of the electromagnetic spectrum; see [16] for commonly used color maps. We provide all these common maps for user selection in our data processing module.

Transfer Function To reveal structure in the image data, we apply transfer function techniques to compute opacity based on user parameters and the image pixel values. This step is necessary to support the volume visualization step to be presented in Section 4.

To provide interactive control of data exploration, we load the converted multiwavelength data into the graphics memory and apply shader programs to carry out the related data processing on the GPU.

4 MULTIWAVELENGTH DATA REPRESENTATIONS

Conceptually, the multiwavelength data set can be viewed as a 4D data volume (with each data sample as a point in 4D space) or a 3D scalar field [20]: 2D for the Galactic coordinates (l, b) (spatial), 1D for the wavelength/frequency (electromagnetic spectrum), and 1D for the flux density (energy per second). In other words, we can regard each data pixel as a point in 4-space. To bring this data set into the visualization, we can intuitively map the galactic coordinates (l, b) to the $X - Y$ dimensions (the image plane) in the data presentation space, and the wavelength dimension to the third spatial dimension perpendicular to this image plane. The 1D flux density values can be color-coded according to the intensity at each 3D point of $(l, b) \times \lambda$ space. Note that in conventional astronomy presentations (see, e.g., [40]), line charts are used with $\log(\text{flux density})$ versus $\log(\text{wavelength})$.

In general, we map the galactic longitude (l), the galactic latitude (b), and the wavelength (in logarithmic scale), to the X , Y , and Z dimensions of the 3D data space (when creating a reference volume texture data), respectively, because mapping the wavelength dimension to a spatial dimension in the data presentation space is an intuitive choice. In this way, we can visually perceive the relative locations of individual multiwavelength image data along

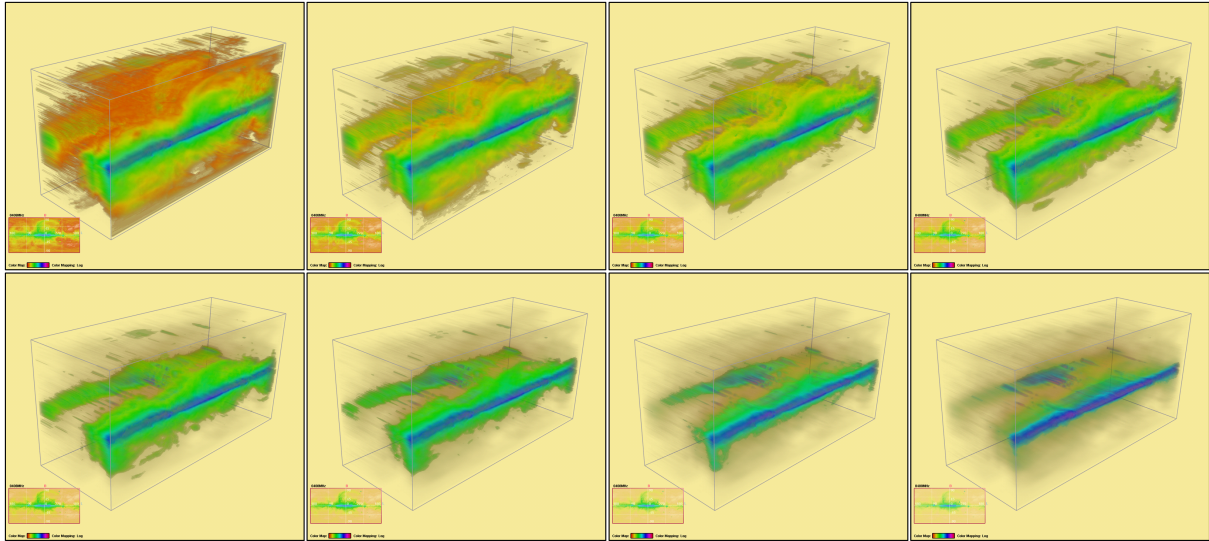


Fig. 4. Volume-rendered model: An image sequence depicting a continuous change in the transfer function (left to right, and then top to bottom).

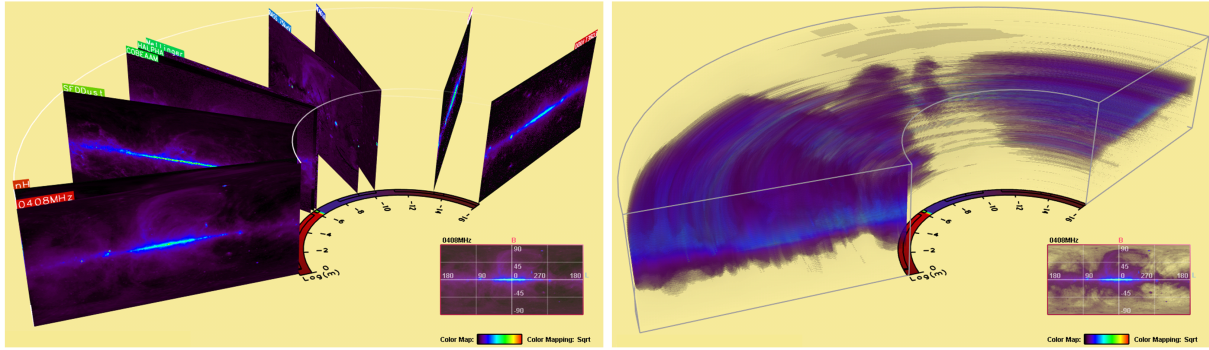


Fig. 5. Horseshoe model. (Left) Combined with textured image-stack model. (Right) Combined with volume-rendered model.

the wavelength dimension; however, it is also possible to swap the role of wavelength and flux density in the presentation mapping, and to visualize the distribution of flux density over wavelength. In summary, to render this data presentation space, we propose to use the following visual representation models:

Image-stack model The image stack is a basic visual model that stacks individual multiwavelength colored-coded images along the third dimension; here, we first use a logarithmic scale for the wavelength dimension (in meters) and arrange the color-coded images at their corresponding locations. Since our data processing pipeline is built on the GPU, we can have interactive data and color mapping as well as transfer function control. Hence we can interactively adjust the pixel opacity according to the flux density range we want to expose. In Figure 3, transparency allows us to see through the images. We can also adjust the range of spectra of interest and only show data within that range. Note that the color bar at the lower left hand side of the images denotes the wavelength dimension in logarithmic scale.

Volume-rendered model Observing the fact that the multiwavelength data volume can be viewed as a 3D scalar function of flux density values, our second visual model re-organizes the data and presents it using volume visualization methods. Since the given allsky surveys do not fully cover the entire wavelength range in the electromagnetic spectrum, we can either interpolate the flux density values (like the 2D line charts used by astronomers: $\log(\text{flux density})$ versus $\log(\text{wavelength})$) across the wavelength dimension or blank out the missing regions in the visualizations, see Figure 4 for the corresponding illustrations. Note that in this visualization model, we can also apply standard interactive volume visualization techniques such as clipping planes and transfer functions.

Horseshoe model Finally, we adopt the horseshoe presentation

model [7, 53] as an alternative to the rectangular box model for stacking the multiwavelength images. With this model, the semi-circular sweep can help to spread out the image data across the wavelength dimension. Note that we can combine the horseshoe model with the textured image-stack model or the volume-rendered model [7] to produce the visualizations; see Figure 5.

5 VISUAL EXPLORATION

Following the data processing pipeline and the data presentation models for displaying the data volumes, the last component in the visualization workflow consists of a set of interactive visual tools for exploring and analyzing the multiwavelength data:

Interactive Data Mapping Our UI controls support interactive adjustment of the following parameters in the data processing pipeline:

1. Data thresholding, clamping the flux density value against a user-specified range
2. Selection of the data mapping scheme: *linear*, *sqrt*, and *log*
3. A checkbox for global or local rescaling
4. Selection of the color map
5. Adjustment of the transfer function

Mini-map Explorer The mini-map explorer is a navigation and visual cue tool consisting of a small window gadget showing the part of the galactic (l, b) space that the input multiwavelength data covers; it has the following three functionalities:

- **Visualizer** – First, it shows on its background the image data (at a particular wavelength) that is selected by the user. When the user tunes the parameters in the data processing pipeline, this background image is altered to reveal the individual effect on the selected image data.

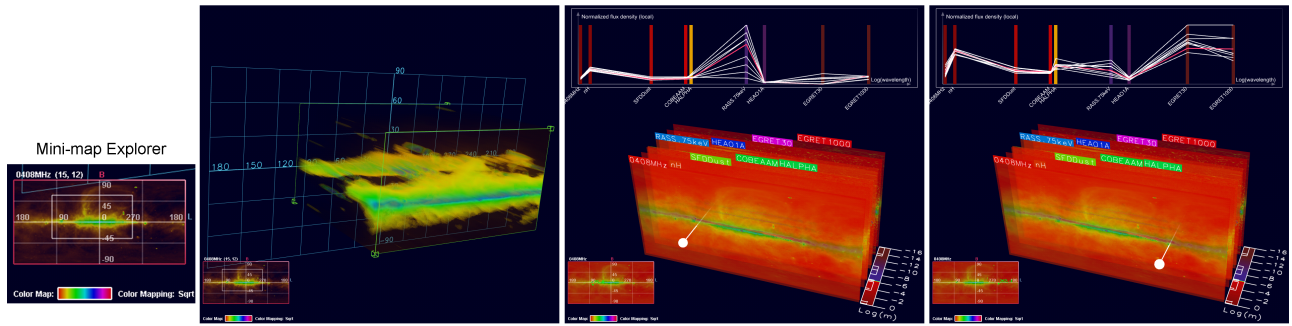


Fig. 6. Using the mini-map explorer to select regions over the galactic $l-b$ coordinate space (left), and to probe the multiwavelength data (right).

- Region selection – Secondly, we can define a bounding region on this mini-map explorer to select a particular region of interest over the (l, b) domain. See Figure 6 (left) for an example.
- Data Probing – Finally, we can click on the mini-map to probe the multiwavelength data at a specific (l, b) . The two sub-figures on the right hand side of Figure 6 show two examples probing Cygnus (left) and the Vela Nebula (right). The plot shown on the top of these two subfigures plot the normalized flux density (in local rescaling mode) against the logarithm of wavelength. Since Cygnus is a strong X-ray source, while Vela Nebula is a strong Gamma-ray source, we see that we can use this probing tool to interactively examine contrasting data. Note that we can also drag the probing point over the mini-map explorer to search over the (l, b) space; this probing tool can interactively sample a 3×3 window of flux densities centered on the probing point. The white line segments correspond to the surrounding data samples, while the red line segments represent the mean values.

Interactive feature analysis The feature analysis toolbox supports exploration of feature correlations in the multiwavelength data. We first select a reference image data set at a certain wavelength; after this selection, the reference data will be shown on the background of the mini-map explorer. Then we can draw (like a paint brush) a mask over the mini-map to outline the feature on the image that we want to explore. After that, the GPU will compute the data correlation between the reference image against each of the other image data within this selected mask. Since the GPU is used for computing the feature correlation, we revert to a distance metric that can be easily programmed to support interactive exploration, typically a Gaussian-weighted SSD (Summed Square Difference). After that, we can further threshold the resulting values and apply color coding to visualize the data correlation. An example is presented in Section 6.

6 IMPLEMENTATION AND RESULTS

6.1 Implementation Details

This subsection details the employed hardware configuration, our software implementation, and also the shader programs we developed.

- The hardware system employed is an HP xw4400 workstation with an Intel Core(TM)2 CPU 6400 running at 2.13GHz with 2GB Memory. We installed two NVidia Geforce 8800 GTX graphics boards, each with 768MB memory (in SLI Mode).
- We implemented the visualization software using OpenGL 2.0 (using the OpenGL shading language, GLSL). We first load the high-dynamic-range multiwavelength data (after data conversion) into the graphics memory as float textures, using the GL extension `GL_LUMINANCE32F_ARB`. Then we apply a series of fragment programs to carry out the data processing pipeline and feed the result to an offscreen buffer (a framebuffer object) for storage before the visualization. When we adjust parameters in the data processing pipeline, we can interactively update this buffer texture and modify the visualizations.
- We use GPU-based ray casting techniques [10] to produce the volume visualizations in both the rectangular box mode and the horseshoe mode. In the horseshoe mode, after we compute the

ray-horseshoe intersection, we require additional shader code to transform the 3D locations inside the horseshoe model to texture coordinates in the framebuffer object (by using the parameters in the semi-circular sweep). These computations can also be done on the GPU, and hence we can employ the same buffer texture (the framebuffer object) in different presentation models.

6.2 Visualization Results

In this subsection, we visualize three different kinds of astronomical objects, including a supernova remnant, a nebula, and a galaxy.

Supernova remnant: Loop I The first example is the supernova remnant called Loop I. This is a very large-scale coherent bubble-like structure that spans over 100 degrees of angular size in the sky; since this thin structure is invisible in the optical range, human observers did not notice it until the development of large radio telescopes. Figure 7 shows a sketch of the 3D position and size of Loop I, published in a recent astronomy article [54], together with an illustration of its appearance in the 408MHz radio survey [23].

Since Loop I is invisible in the optical range, multiwavelength imaging is needed to reveal and study this interesting structure. Typically, if we look at the northern portion of the sky in the radio spectrum, we can find the prominent structure of Loop I, as shown on the right hand side of Figure 7. Now, if employ our visualization system and select the 408MHz radio survey as the reference (refer to Figure 8), we can interactively draw a mask on the mini-map explorer to highlight the Loop-I region on the radio survey. The GPU can then instantaneously compute Gaussian-weighted SSD over the masked region and display the SSD values over all other wavelength images (refer to the right hand side of Figure 8). With the GPU support, such a visual exploration can be performed at interactive speeds and we can progressively modify the mask, the color map for the SSD values, and also the parameters in the data processing pipeline.

The Crab Nebula The Crab Nebula is detectable as a variety of structures appearing in many different wavelengths (see, e.g., [5]). Images of the Crab derived from several different data sets can be displayed in our system, as shown in Figure 9 (top). Here we show an image-stack model and a volume-rendered model, and then cut through the volume-rendered model to unveil the flux density variation inside; original false color multiwavelength images produced by various astronomy groups are shown below for reference.

The Andromeda Galaxy Galaxies are another natural target for multiwavelength examination. Andromeda, the Milky Way's sister galaxy, can be seen in multiple aspects using our system, as shown in Figure 10. Here, we can see that Andromeda's spiral arm is a stronger source of radiation relative to its disk. We note that since there is a large gap between the radio and far-infrared spectral ranges, the flux density interpolation fills the frontal part of the volume rendering mostly with the radio spectrum data, and hence produces finger-like shapes in the volume renderings.

Since different images have been acquired by diverse astronomy research groups, the raw images may not be well-aligned with each other; further image alignment [14] is needed, for example, to generate compatible data sets for the multiwavelength data of the Crab nebula and the Andromeda galaxy.

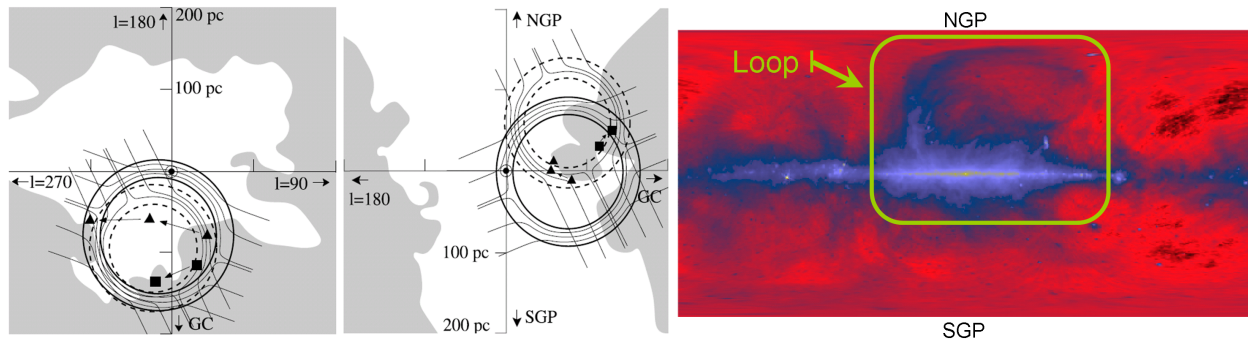


Fig. 7. Left: sketch of the Loop I model in interstellar space, courtesy of Wolleben [54]. In this sketch, l is the galactic longitude (see Figure 2); GC stands for the direction to the galactic center (the Milky Way center is $l = 0$); NGP and SGP refer to north galactic pole and south galactic pole, respectively, while pc denotes distance in parsecs, where 1 parsec = 3.262 light-years; Right: Loop I in the allsky radio survey at 408MHz.

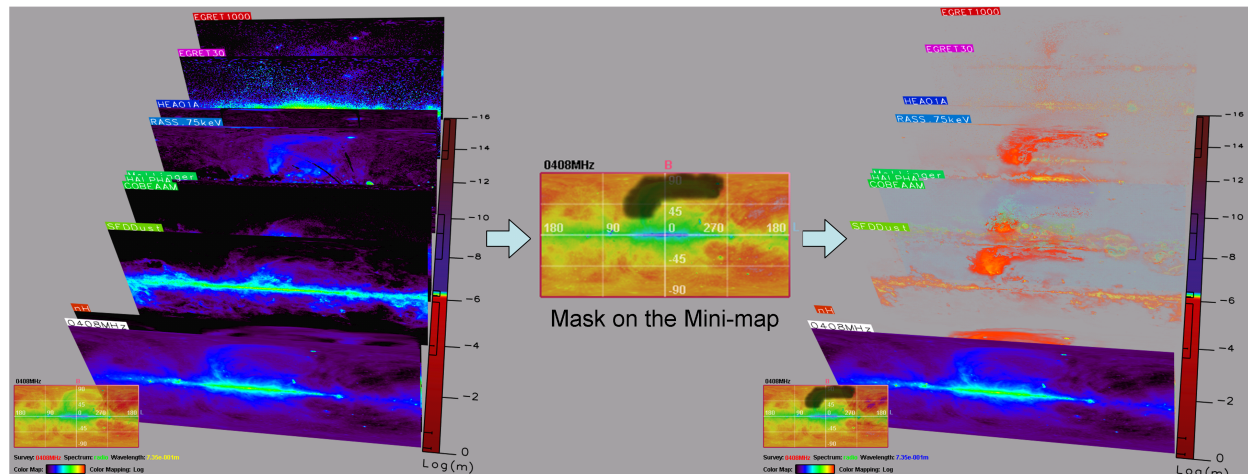


Fig. 8. A Visualization Example: Highlighting the Loop-I structure by a mask interactively drawn by the user on the mini-map.

7 CONCLUSION

This paper proposes a comprehensive visualization workflow to address the visualization of multiwavelength astronomical data. Supporting a uniform visualization environment for a wide variety of multiwavelength astronomical data opens a new window into the study of these data collected from the sky. In our workflow, three major components are offered: GPU-based data processing, new ways of visualizing the multiwavelength astronomical data including volume visualization and the horseshoe model, and a collection of interactive visual exploration tools tailored for both examining and analyzing the multiwavelength data volume. Three examples of multiwavelength data exploration were presented using this workflow architecture: the supernova remnant called Loop I in the allsky data, the Crab nebula, and the Andromeda galaxy.

Future work As a succeeding development, we plan to construct an integrated visualization architecture that considers not only the multiwavelength data, but also three-dimensional spatial data (distances to stars, galaxies, intergalactic clouds, etc.) as well as sketched 3D models, such as Loop I and the local bubble, in the interstellar environment to provide integrated visualizations with the largest possible variety of scientific data.

Acknowledgments We would like to express our gratitude to our astronomy collaborator, Priscilla Frisch, for her endless support, insightful suggestions, and proofreading, to Tom McGlynn for his guidance in the data conversion, and also to the anonymous reviewers for providing the useful discussions and comments that helped to improve the paper. This research was supported by the Research Grants Council of the Hong Kong Special Administrative Region, under RGC Earmarked Grant (Project No. HKUST612505 and HKUST618208).

REFERENCES

- [1] G. V. G. Baranoski, J. G. Rokne, P. Shirley, T. Trondsen, and R. Bastos. Simulating the Aurora Borealis. In *Proc. of Pacific Graphics 2000*, pages 2–14, Oct. 2000.
- [2] D. S. Birney, G. Gonzalez, and D. Oesper. *Observational Astronomy*. Cambridge University Press, 2nd edition, July 2006.
- [3] J. Blinn. Voyager Fly-by Animations, 1977–1987. Animations depicting space missions to Jupiter, Saturn and Uranus: <http://research.microsoft.com/users/blinn/FLYBY.HTM>.
- [4] E. W. Brugel, G. O. Domik, and T. R. Ayres. Visualization techniques to aid in the analysis of multi-spectral astrophysical data sets. Technical report, Sept. 1993. Colorado University Report.
- [5] Caltech's Infrared Astronomy Center. The multiwavelength astronomy gallery. website: http://coolcosmos.ipac.caltech.edu/cosmic_classroom/multiwavelength_astronomy/multiwavelength_museum.
- [6] A. N. Cox. *Allen's Astrophysical Quantities*. Springer/Verlag, 2000.
- [7] G. Daniel and M. Chen. Video visualization. In *IEEE Visualization Conference 2003*, pages 409–416, 2003.
- [8] J. M. Dickey and F. J. Lockman. H I in the galaxy. *Annual Review of Astron and Astrophys*, 28:215–261, 1990.
- [9] C. Emmart, D. R. Nadeau, J. Genetti, and E. Wesselak. Volume Visualization of the Orion Nebula, 2000. SIGGRAPH 2000 Electronic Theatre, Issue 134: <http://vis.sdsc.edu/research/orion.html>.
- [10] K. Engel, M. Hadwiger, J. Kniss, C. Rezk-Salama, and D. Weiskopf. *Real-time Volume Graphics*. A K Peters, 2006.
- [11] European Space Agency (ESA). Infrared space observatory (ISO). website: <http://iso.esac.esa.int>.
- [12] D. P. Finkbeiner. A Full-Sky H-alpha Template for Microwave Foreground Prediction. *Astrophysical Journal Supplement Series*, 146(2):407–415, 2003.
- [13] E. O. for Astronomical Research in the Southern Hemisphere (ESO). Very large telescope project. website: <http://www.eso.org/projects/vlt>.
- [14] C.-W. Fu and A. J. Hanson. A transparently scalable visualization architecture for exploring the Universe. *IEEE Tran. on Visualization and Computer Graphics*, 13(1):108–121, 2007.
- [15] J. D. Genetti. Volume-rendered galactic animations. *Communications of the ACM*, 45(11):62–66, 2002.
- [16] Goddard space flight center, NASA. Multiwavelength Milky Way web

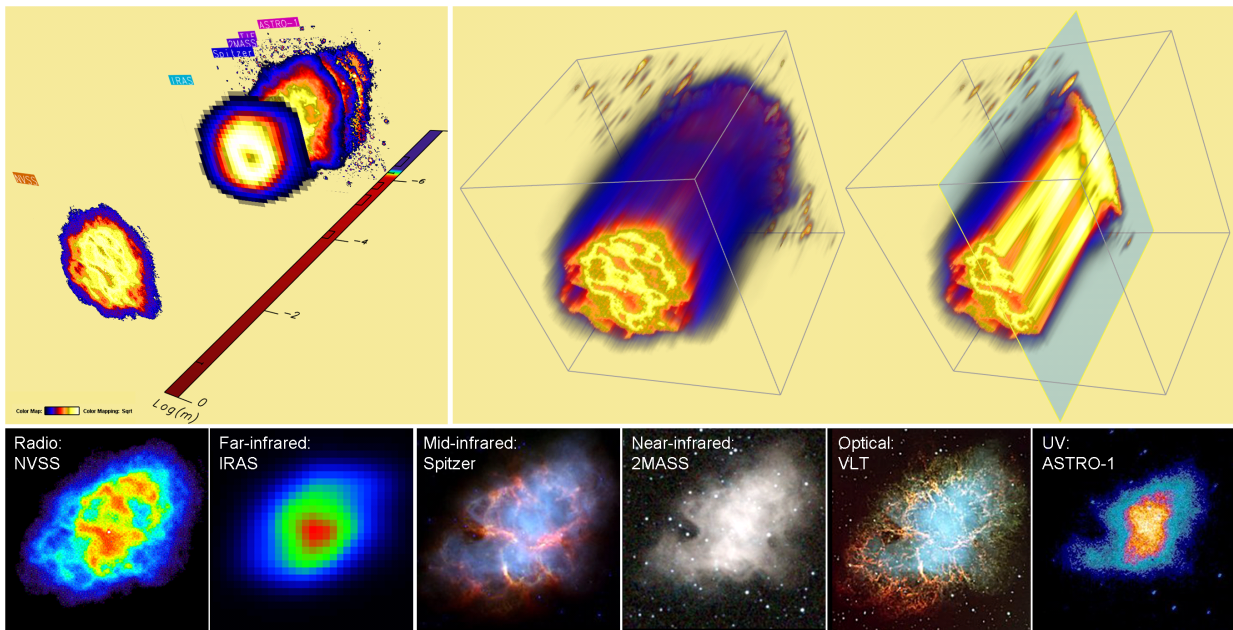


Fig. 9. A Visualization Example: Multiwavelength Crab nebula; Survey data employed include: the NRAO VLA Sky Survey (NVSS) [45] for radio, IRAS (from Infrared Processing and Analysis Center, Caltech/JPL. IPAC is NASA's Infrared Astrophysics Data Center) [30] for far-infrared, Spitzer Space Telescope Data (Credit: NASA/JPL-Caltech/R. Gehrz (University of Minnesota)) [44] for Mid-infrared, the Two Micron All Sky Survey (2MASS) [49] for near-infrared (note: the atlas Image obtained as part of the Two Micron All Sky Survey (2MASS), a joint project of the University of Massachusetts and the Infrared Processing and Analysis Center/California Institute of Technology, funded by the National Aeronautics and Space Administration and the National Science Foundation), the Very Large Telescope Project [13] (Credit: FORS Team, 8.2-meter VLT, ESO) for Optical, and ASTRO-1 mission [26] for UV.

- pages, 2005. <http://mwmw.gsfc.nasa.gov>.
- [17] R. Gooch. Astronomers and their shady algorithms. In *IEEE Visualization Conference 1995*, pages 374–377. IEEE, October/November 1995.
- [18] A. J. Hanson and C.-W. Fu. Cosmic Clock, 2000. SIGGRAPH Video Review, vol. 134, scene 5.
- [19] A. J. Hanson, C.-W. Fu, and E. A. Wernert. Visualizing cosmological time. In F. H. Post, G. M. Nielson, and G.-P. Bonneau, editors, *Data Visualization: The State of the Art*, pages 423–438. Kluwer academic publishers, May 21–26, 2000, Dagstuhl, DE, 2003.
- [20] A. J. Hanson and P. A. Heng. Four-dimensional views of 3D scalar fields. In *IEEE Visualization Conference 1992*, pages 84–91. IEEE Computer Society Press, 1992.
- [21] R. C. Hartman, D. L. Bertsch, S. D. Bloom, A. W. Chen, P. Deines-Jones, J. A. Esposito, C. E. Fichtel, D. P. Friedlander, S. D. Hunter, L. M. McDonald, P. Sreekumar, and D. J. Thompson. The third EGRET catalog of high-energy Gamma-ray sources. *Astrophysical Journal Supplement Series*, 123:79–202, 1999.
- [22] D. Hartmann and W. B. Burton. *Atlas of Galactic Neutral Hydrogen*. Cambridge University Press, Cambridge, 1997.
- [23] C. G. T. Haslam, H. Stoffel, C. J. Salter, and W. E. Wilson. A 408 MHz all-sky continuum survey. II - The atlas of contour maps. *Astronomy and Astrophysics, Supplement*, 47:1, 1982.
- [24] M. G. Hauser, R. G. Arendt, T. Kelsall, E. Dwek, N. Odegard, J. L. Weiland, H. T. Freudenreich, W. T. Reach, R. F. Silverberg, S. H. Moseley, Y. C. Pei, P. Lubin, J. C. Mather, R. A. Shafer, G. F. Smoot, R. Weiss, D. T. Wilkinson, , and E. L. Wright. The COBE diffuse infrared background experiment search for the cosmic infrared background. I. limits and detections. *Astrophysical Journal*, 508:25–43, Nov. 1998.
- [25] M. Haverkorn, P. Katgert, and A. G. de Bruyn. Structure in the polarized galactic synchrotron emission, in particular “depolarization canals”. *Astronomy and Astrophysics*, 427:549–559, 2004.
- [26] G. S. Hennessy, R. W. O’Connell, K. P. Cheng, R. C. Bohlin, N. R. Collins, T. R. Gull, P. Hintzen, J. E. Isensee, W. B. Landsman, M. S. Roberts, A. M. Smith, E. P. Smith, and T. P. Stecher. Ultraviolet imaging telescope observations of the Crab nebula. *Astrophysical Journal, Part 2 - Letters*, 395(1):L13–L16, 1992.
- [27] M. Hopf, M. Luttenberger, and T. Ertl. Hierarchical splatting of scattered 4D data. *IEEE Computer Graphics and App.*, 24(4):64–72, 2004.
- [28] J. Jacob and L. Plesea. Fusion, visualization and analysis framework for large, distributed data set. In *IEEE Proceedings on Aerospace Confer-*
- ence, 2001*, volume 7, pages 3523–3530, 2001.
- [29] H. W. Jensen, F. Durand, J. Dorsey, M. M. Stark, P. Shirley, and S. Premoze. A physically-based night sky model. In *Proc. of ACM SIGGRAPH 2001*, pages 399–408, Aug. 2001.
- [30] Jet Propulsion Laboratory, California Institute of Technology. Infrared Astronomical Satellite (IRAS), NASA/IPAC Infrared Science Archive. website: <http://irsa.ipac.caltech.edu/index.html>.
- [31] R. Kahler, D. Cox, R. Patterson, S. Levy, H.-C. Hege, and T. Abel. Rendering the first star in the Universe - a case study. In *IEEE Visualization Conference 2002*, pages 537–540, 2002.
- [32] C. Kramer. Spatial response - contribution to the framework document of HIFI/Herschel space observatory. Technical report, 2003.
- [33] H. Li, C.-W. Fu, Y. Li, and A. J. Hanson. Visualizing large-scale uncertainty in astrophysical data. *IEEE Tran. on Visualization and Computer Graphics*, 13(6):1640–1647, 2007.
- [34] Y. Li, C.-W. Fu, and A. J. Hanson. Scalable WIM: Effective exploration in large-scale astrophysical environments. *IEEE Tran. on Visualization and Computer Graphics*, 12(5):1005–1011, 2006.
- [35] M. Magnor, K. Hildebrand, A. Lintu, and A. J. Hanson. Reflection nebula visualization. In *IEEE Visualization Conference 2005*, pages 255–262, Oct. 2005.
- [36] M. Magnor, G. Kindlmann, and C. Hansen. Constrained inverse volume rendering for planetary nebulae. In *IEEE Visualization Conference 2004*, pages 83–90, Oct. 2004.
- [37] Max-Planck-Institute for Radio astronomy. The Effelsberg 100-m radio telescope. website: http://www.mpifr-bonn.mpg.de/div/effelsberg/index_e.html.
- [38] T. McGlynn, K. Scollick, and N. White. SkyView: The multi-wavelength sky on the Internet, McLean, B.J. et al., new horizons from multi-wavelength sky surveys, 1996. Kluwer Academic Publishers, 1996, IAU Symposium No. 179, p465. website: <http://skyview.gsfc.nasa.gov>.
- [39] A. Mellinger. A $360^\circ \times 180^\circ$ all-sky panorama., 2000. available at <http://home.arcor-online.de/axel.mellinger>.
- [40] H. Meyer. Photons from the Universe - new frontiers in astronomy. 1997. 14 pages, invited talk at the Gamma-Gamma conference “Photon ’97”.
- [41] J. Miller, C. W. Quammen, and M. C. Fleenor. Interactive visualization of intercluster galaxy structures in the horologium-reticulum supercluster. *IEEE Tran. on Visualization and Computer Graphics*, 12(5):1149–1156, 2006.

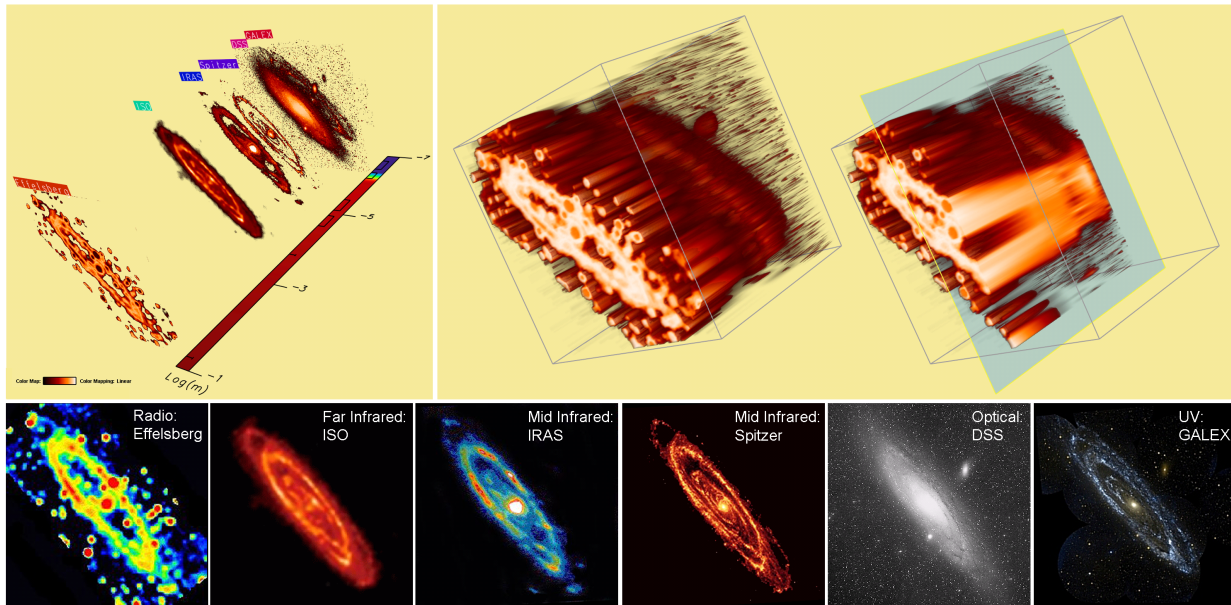


Fig. 10. A Visualization Example: Multiwavelength Andromeda Galaxy (M31); Survey data employed include: the Effelsberg 100-m radio telescope data [37] for radio, Infrared Space Observatory (Credit: ESA/ISO/ISOPHOT and M. Haas et al.) [11] for infrared, IRAS (from Infrared Processing and Analysis Center, Caltech/JPL. IPAC is NASA's Infrared Astrophysics Data Center) [30] for far-infrared, Spitzer Space Telescope Data (Credit: NASA/JPL-Caltech/R. Gehrz (University of Minnesota)) [44] for mid-infrared, Digitized Sky Survey (Credit: Space Telescope Science Institute under U.S. Govt. grant NAG W-2166) [51] for optical, and UV data from the Galaxy Evolution Explorer (GALEX) mission (Credit: NASA/JPL-Caltech) [43].

- [42] D. R. Nadeau, J. D. Genetti, S. Napear, B. Pailthorpe, C. Emmart, E. Wesselak, and D. Davidson. Visualizing Stars and Emission Nebulae. *Computer Graphics Forum*, 20(1):27–33, Mar. 2001. Also in Eurographics 2000 (short presentations).
- [43] NASA/JPL and Caltech. Galaxy Evolution Explorer (GALEX). website: <http://www.galex.caltech.edu>.
- [44] NASA/JPL-Caltech/R. Gehrz. Spitzer space telescope data. website: <http://irsa.ipac.caltech.edu/applications/Spitzer/Spitzer>.
- [45] National Radio Astronomy Observatory. NRAO VLA Sky Survey (NVSS). website: <http://www.vla.nrao.edu>.
- [46] P. Navratil, J. Johnson, and V. Bromm. Visualization of cosmological particle-based datasets. *IEEE Tran. on Visualization and Computer Graphics*, 13(6):1712–1718, 2007.
- [47] J. P. Ostriker and M. L. Norman. Cosmology of the early Universe viewed through the new infrastructure. *Communications of the ACM*, 40(11):84–94, Nov. 1997.
- [48] D. J. Schlegel, D. P. Finkbeiner, and M. Davis. Maps of dust infrared emission for use in estimation of reddening and cosmic microwave background radiation foregrounds. *Astrophysical Journal*, 500:525, 1998.
- [49] M. Skrutskie, R. Cutri, R. Stiening, M. Weinberg, S. Schneider, J. Carpenter, C. Beichman, R. Capps, T. Chester, J. Elias, J. Huchra, J. Liebert, C. Lonsdale, D. Monet, S. Price, P. Seitzer, T. Jarrett, J. Kirkpatrick, J. Gizis, E. Howard, T. Evans, J. Fowler, L. Fullmer, R. Hurt, R. Light, E. Kopan, K. Marsh, H. McCallon, R. Tam, S. V. Dyk, and S. Wheelock. The Two Micron All Sky Survey (2MASS). *Astronomical Journal*, 131(2):1163–1183, 2006. website: <http://www.ipac.caltech.edu/2mass>.
- [50] S. L. Snowden, M. J. Freyberg, P. P. Plucinsky, J. H. M. M. Schmitt, J. Truemper, W. Voges, R. J. Edgar, D. McCammon, and W. T. Sanders. First maps of the soft X-ray diffuse background from the ROSAT XRT/PSPC all-sky survey. *Astrophysical Journal*, 454:643–653, Dec. 1995.
- [51] Space Telescope Science Institute (STScI). Digitized Sky Survey (DSS). website: <http://archive.stsci.edu/dss>.
- [52] D. Weiskopf, M. Borchers, T. Ertl, M. Falk, O. Fechtig, R. Frank, F. Rude, A. King, U. Kraus, T. Muller, H.-P. Nollert, I. Mendez, H. Ruder, T. Schafnitzel, S. Schar, C. Zahn, and M. Zatloukal. Visualization of cosmological particle-based datasets. *IEEE Tran. on Visualization and Computer Graphics*, 12(4):522–534, 2006.
- [53] A. S. Winter and M. Chen. Image-swept volumes. *Computer Graphics Forum*, 1(3):441–450, 2002.
- [54] M. Wolleben. A new model for the Loop I (North polar spur) region. *The*

Astrophysical Journal, 664:349–356, 2007.

Appendix: converting multiwavelength data

Since techniques for measuring different frequency bands in the EM spectrum result in different physical units, we need the following formulas to convert the data values to common units:

- Conversion between wavelength λ (m) and frequency ν (Hz)

$$c = \lambda \nu,$$
 where c is the speed of light in vacuum ($\sim 2.9979 \times 10^8$ in m/s).
- The energy E (eV) of a particle with frequency ν (Hz) is

$$E = h\nu,$$
 where h is Planck's constant ($4.13566733 \times 10^{-15}$ in $eV \cdot s$, electron-Volt-seconds).
- Conversion between temperature (degrees Kelvin, K) and flux density (Janskys, Jy)

The conversion from antenna temperature in degrees Kelvin (in radio astronomy) to flux density in Janskys (Jy) is detailed in [32]. The conversion depends on the telescope diameter and aperture efficiency; in practice, we use the conversion factor in [25]: $1mJy/bm = 0.127K$.
- Conversion between flux density per steradian (Jy/sr) and energy (eV)

By definition, $1MJy$ (MegaJanskys) $= 1Wm^{-2}Hz^{-1} \times 10^{-20}$, and $1kW-hour = 2.247 \times 10^{25}eV$. Thus we can first determine the effective detection area of the related device, combine these two definitions, and convert between flux density and energy. In addition, we also have to normalize the pixel data by the solid angle (in steradians) of each pixel.
- Conversion between luminous power in Rayleighs (R) and energy in electron-Volts (eV)

By definition, $1R = \frac{1}{4\pi} \times 10^{10} \text{photons } s^{-1}m^{-2}sr^{-1}$, so we can first apply $E = h\nu$ to compute the energy of a photon in electron-Volts, and then normalize the result by using the solid angle and effective detection area as above.
- Note: the allsky Mellinger image for the optical portion of the electromagnetic spectrum is uncalibrated, and hence, we can only show it in the image stack model, but not the others.